REPORT DOCUMENTATION PAGE

Form Approved OMB NO. 0704-0188

1. REPORT DATE (DD-MM-YYYY)	2. REPORT TYPE	3. DATES COVERED (From - To)
	New Reprint	-

4. TITLE AND SUBTITLE
A down-valley low-level jet event during T-REX 2006

5a. CONTRACT NUMBER
W911NF-09-1-0441

5b. GRANT NUMBER

5c. PROGRAM ELEMENT NUMBER
611102

6. AUTHORS
Sen Chiao, Robert Dumais

5d. PROJECT NUMBER

5e. TASK NUMBER

5f. WORK UNIT NUMBER

7. PERFORMING ORGANIZATION NAMES AND ADDRESSES
Florida Institute of Technology
150 West University Blvd.

Melbourne, FL 32901 -6975

8. PERFORMING ORGANIZATION REPORT NUMBER

9. SPONSORING/MONITORING AGENCY NAME(S) AND ADDRESS (ES)
U.S. Army Research Office
P.O. Box 12211
Research Triangle Park, NC 27709-2211

10. SPONSOR/MONITOR'S ACRONYM(S)
ARO

11. SPONSOR/MONITOR'S REPORT NUMBER(S)
54155-EV.11

12. DISTRIBUTION AVAILIBILITY STATEMENT
Approved for public release; distribution is unlimited.

13. SUPPLEMENTARY NOTES
The views, opinions and/or findings contained in this report are those of the author(s) and should not contrued as an official Department of the Army position, policy or decision, unless so designated by other documentation.

14. ABSTRACT
A prolonged down-valley flow and low-level jet was observed throughout the Enhanced Observing Period 4 (Apr 28-29) of the 2006 Terrain-induced Rotor Experiment, held in the Owens Valley of California near the town of Independence. The low-level jet was strongest during the nocturnal hours, and special field observations captured important details of the event lifecycle. High resolution simulations using the Weather Research and Forecasting numerical weather prediction (NWP) model were generated, with

15. SUBJECT TERMS
WRF, PBL, T-REX

16. SECURITY CLASSIFICATION OF:			17. LIMITATION OF ABSTRACT	15. NUMBER OF PAGES	19a. NAME OF RESPONSIBLE PERSON
a. REPORT	b. ABSTRACT	c. THIS PAGE			George Maul
UU	UU	UU	UU		19b. TELEPHONE NUMBER: 321-674-7453

Report Title

A down-valley low-level jet event during T-REX 2006

ABSTRACT

A prolonged down-valley flow and low-level jet was observed throughout the Enhanced Observing Period 4 (Apr 28-29) of the 2006 Terrain-induced Rotor Experiment, held in the Owens Valley of California near the town of Independence. The low-level jet was strongest during the nocturnal hours, and special field observations captured important details of the event lifecycle. High resolution simulations using the Weather Research and Forecasting numerical weather prediction (NWP) model were generated, with underlying assumptions being that model resolution, boundary layer physics, and nesting configuration would be dominant controlling factors in reproducing the jet. The large-scale conditions were dry throughout the event, so moist physics were not a significant forcing consideration. For the control simulation, a two-nest (4.5 km and 1.5 km grid spacing) configuration with 90 vertical levels was applied. Additionally, the Quasi-Normal Scale Elimination planetary boundary and surface layer option was selected due to its published performance under conditions of stable stratification. Three other sensitivity simulations were run for comparison, differing from the control just in the choice of vertical resolution (60 versus 90 levels with Quasi-Normal Scale Elimination) and planetary boundary/surface layer physics (90 levels/Mellor-Yamada-Jancic; 90 levels/Yonsei State University). Although the gross evolution (location, height, and timing) of the low-level jet is captured by all model runs (with the 1.5 km inner nest providing the more accurate details), there were at times large underestimations of the nocturnal jet speed max in each simulation (approaching 100% error, or up to almost 10 m s-1). Overall, the variations of vertical resolution and planetary boundary/surface physics against the control seemed to (1) yield little overall improvement to statistical or subjective evaluations; (2) do little to improve deficiencies in reproducing the magnitude strength of the nocturnal down-valley low-level jet. Since the cold-start simulations spanned 36-h (including a 12-h spin-up period), it was suspected that the lateral boundary conditions imposed on the outermost 4.5 km nest might negatively impact the interior model solutions in the Owens Valley. To investigate this possibility, an additional simulation was executed by adding two extra nests to the control configuration: an outer 13.5 km and an inner 500 m. This simulation produced a better evolution of the nocturnal low-level jet and especially the speed max. The addition of the larger 13.5 km nest appears more critical to this improvement than that of the extra spatial resolution provided by the inner 500 m nest, which supports the idea that accurate capturing of the large-scale synoptic condition was critical in reproducing important details of this down-valley low-level jet event. The extra 500 m resolution did seem to improve the morning valley cold pool forecast.

REPORT DOCUMENTATION PAGE (SF298)
(Continuation Sheet)

Continuation for Block 13

ARO Report Number 54155.11-EV
A down-valley low-level jet event during T-REX ...

Block 13: Supplementary Note

Approved for public release; distribution is unlimited.

A down-valley low-level jet event during T-REX 2006

Sen Chiao & Robert Dumais

Meteorology and Atmospheric Physics

ISSN 0177-7971

Meteorol Atmos Phys
DOI 10.1007/s00703-013-0279-z

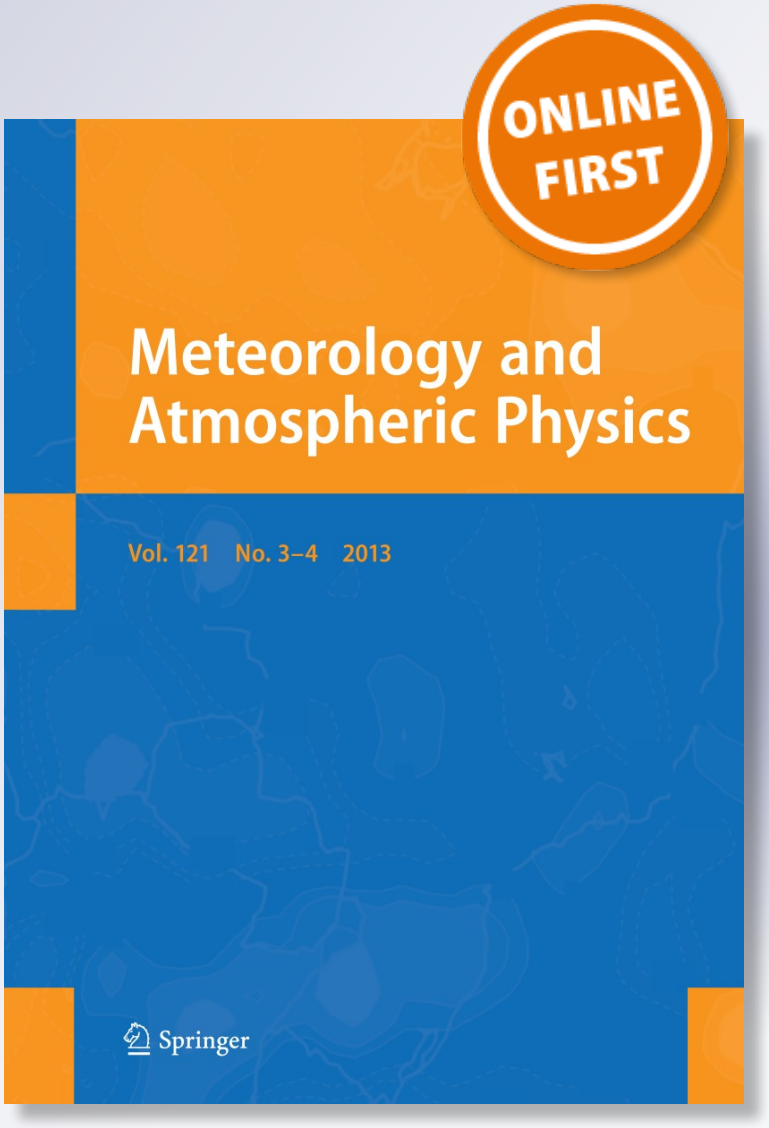

Springer

Meteorol Atmos Phys
DOI 10.1007/s00703-013-0279-z

ORIGINAL PAPER

A down-valley low-level jet event during T-REX 2006

Sen Chiao · Robert Dumais Jr.

Received: 28 April 2013 / Accepted: 20 August 2013

Abstract A prolonged down-valley flow and low-level jet were observed throughout the Enhanced Observing Period 4 (April 28–29) of the 2006 Terrain-induced Rotor Experiment, held in the Owens Valley of California near the town of Independence. The low-level jet was strongest during the nocturnal hours, and special field observations captured important details of the event lifecycle. High-resolution simulations using the Weather Research and Forecasting numerical weather prediction model were generated, with underlying assumptions being that model resolution, boundary layer physics, and nesting configuration would be dominant controlling factors in reproducing the jet. The large-scale conditions were dry throughout the event, so moist physics were not a significant forcing consideration. For the control simulation, a two-nest (4.5 and 1.5 km grid spacing) configuration with 90 vertical levels was applied. Additionally, the Quasi-Normal Scale Elimination planetary boundary and surface layer option were selected due to its published performance under conditions of stable stratification. Three other sensitivity simulations were run for comparison, differing from the control just in the choice of vertical resolution (60 versus 90 levels with Quasi-Normal Scale Elimination) and planetary boundary/surface layer physics (90 levels/Mellor-Yamada-Jancic; 90 levels/Yonsei State University). Although the gross evolution (location, height, and timing) of the low-level jet is captured by all model runs (with the 1.5 km inner nest providing the more accurate details), there were at times large underestimations of the nocturnal jet speed max in each simulation (approaching 100 % error, or up to almost 10 m s^{-1}). Overall, the variations of vertical resolution and planetary boundary/surface physics against the control seemed to (1) yield little overall improvement to statistical or subjective evaluations; (2) do little to improve deficiencies in reproducing the magnitude strength of the nocturnal down-valley low-level jet. Since the cold-start simulations spanned 36 h (including a 12-h spin-up period), it was suspected that the lateral boundary conditions imposed on the outermost 4.5 km nest might negatively impact the interior model solutions in the Owens Valley. To investigate this possibility, an additional simulation was executed by adding two extra nests to the control configuration: an outer 13.5 km and an inner 500 m. This simulation produced a better evolution of the nocturnal low-level jet and especially the speed max. The addition of the larger 13.5 km nest appears more critical to this improvement than that of the extra spatial resolution provided by the inner 500 m nest, which supports the idea that accurate capturing of the large-scale synoptic condition was critical in reproducing important details of this down-valley low-level jet event. The extra 500-m resolution did seem to improve the morning valley cold pool forecast.

Responsible editor: M. Kaplan.

S. Chiao (✉)
Department of Meteorology and Climate Science, San Jose State University, San Jose, CA 95192-0104, USA
e-mail: sen.chiao@sjsu.edu

R. Dumais Jr.
The US Army Research Laboratory, White Sand Missile Range, New Mexico, NM, USA

1 Introduction

The diurnal evolution of mountain-valley flow regimes can be complex and continues to be analyzed by researchers, focusing upon special field study exercises such as the

Published online: 04 September 2013

2006 Terrain-induced Rotor Experiment (T-REX) and the 2000 Vertical Transport and Mixing Experiment (VTMX). Details of the T-REX field experiment can be found in Grubišic et al. (2008), while those of the VTMX in Doran et al. (2002). The T-REX field campaign was held during March and April of 2006, with the primary objective being to study the coupled mountain-wave, rotor, and boundary layer system under highly perturbed atmospheric states. However, there was also a secondary goal to evaluate the structure and evolution of the complex terrain boundary layer during dry quiescent conditions and stable stratification.

The numerical simulation of valley flow under conditions of stable stratification remains a challenging task due to the variability of individual valley locations/geometries/orientations, overlying synoptic forcing, and surface conditions (land cover/vegetation, soil moisture, snow cover, sidewall slopes, etc.). Modeling studies by Whiteman and Zhong (2008), Zhong and Whiteman (2008), and Papadopoulos and Helmis (1999) all examined how the various terms in the momentum and energy equations contributed to aspects of drainage flow evolution and its variation on slopes in valley environments. Drainage winds that develop early in the evening along the valley sidewalls tend to precede and later contribute to the development of a more general down-valley wind regime later at night (Princevac et al. 2008).

The thermal structure of nocturnal valley atmospheres has been elucidated in observational studies by Triantafyllou et al. (1995) and Whiteman et al. (1996), while nocturnal airflow in valleys has been widely observed: Clements et al. (1989), Gudiksen and Shearer (1989), and Mursch-Radlgruber (1995). The depth and magnitude of down-valley flows are also related to the size of the drainage source regions, and these flows may interact with other boundary layer mesoscale circulations such as lake breezes (Zumpfe and Horel 2007).

Banta et al. (2004) summarized the nocturnal low-level jet (LLJ) observed in the Great Salt Lake area and found that local drainage flows and a larger basin jet usually coexist. This results in local regions of convergence and divergence within the valley. The VTMX field experimental study of Pinto et al. (2006) revealed that a valley LLJ can initiate abrupt warming at low-levels due to downward mixing and vertical transport of warm air in the inversion layer just above the surface. Maximum valley LLJ winds often occur within 150 m of the surface. Further evidence of surface LLJ-induced warming is found in the study of Whiteman et al. (2009) from a network of sensors deployed during the T-REX.

In this study, we focus our investigation upon the extended down-valley LLJ event of the T-REX Enhanced Observing Period 4 (EOP4) within the Owens Valley of California. During EOP4 (April 28–29, 2006), the synoptic forcing was strong enough to contribute to the evolution of the LLJ structure. This paper seeks to extend the growing knowledge base obtained from previous T-REX flow studies made during the EOPs, such as Schmidli et al. (2007, 2009). These past studies have found that the strength and vertical structure of the down-valley wind system varied between the EOPs (of which there were five), and was driven strongly through a combination of local valley thermodynamics and mid-level synoptic pressure gradient. These recent T-REX studies are what inspired us to investigate the impact of the different model configurations, boundary layer physics, and resolutions on the EOP4 down-valley LLJ evolution.

The numerical model used in our simulations is the Advanced Research version of the Weather Research and Forecasting (WRF-ARW, hereafter referred to as WRF) model version 3 (Skamarock et al. 2008), and it is applied in a limited-area configuration consistent with that being explored at the U.S. Army Research Laboratory (ARL) for rapid update cycle nowcasting applications (Dumais and Reen 2013; Pattantyus and Dumais 2013). A better prediction of valley wind systems is certainly important to military communities (i.e., transport and dispersion, chemical and pollutant releases, low-level aircraft, tethered platform operations, etc.). The primary goal of this paper is to apply a limited-area WRF configuration(s) similar to that being adopted by ARL, and investigate how well the EOP4

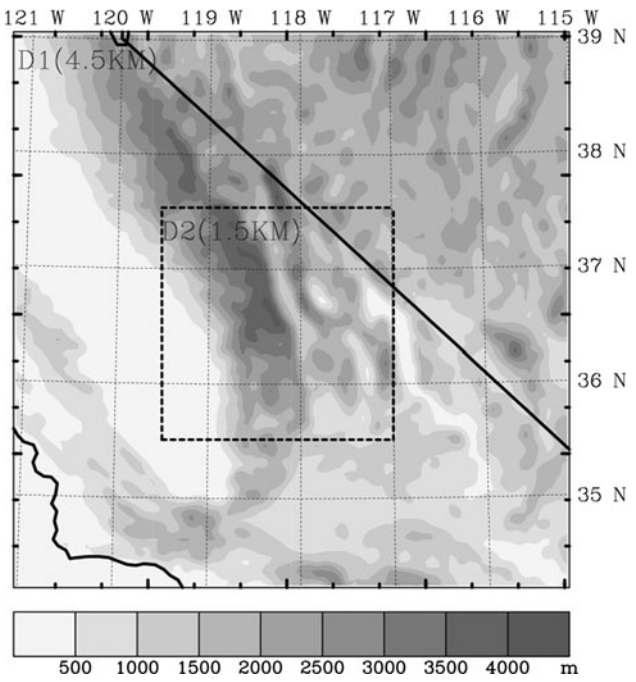

Fig. 1 Domains for numerical simulations used in this study. The grid increments for the two nested meshes are 4.5 and 1.5 km, respectively

Table 1 Model vertical resolution from level 1 to 25 for the 60 and 90 levels configurations

Model half-sigma level	Height agl (60 levels)	Height agl (90 levels)
1	25.87	17.16
2	77.71	51.15
3	129.32	85.26
4	181.56	119.46
5	235.69	153.38
6	292.15	187.81
7	350.97	222.79
8	411.77	257.90
9	475.85	293.57
10	543.68	330.21
11	614.91	367.40
12	690.90	405.16
13	772.15	443.90
14	858.79	483.64
15	951.81	524.37
16	1,052.29	565.70
17	1,161.33	608.04
18	1,279.60	651.83
19	1,407.83	696.66
20	1,547.26	742.98
21	1,698.75	791.23
22	1,863.71	841.01
23	2043.19	892.33
24	2,238.4	945.66
25	2,450.21	1,001.02

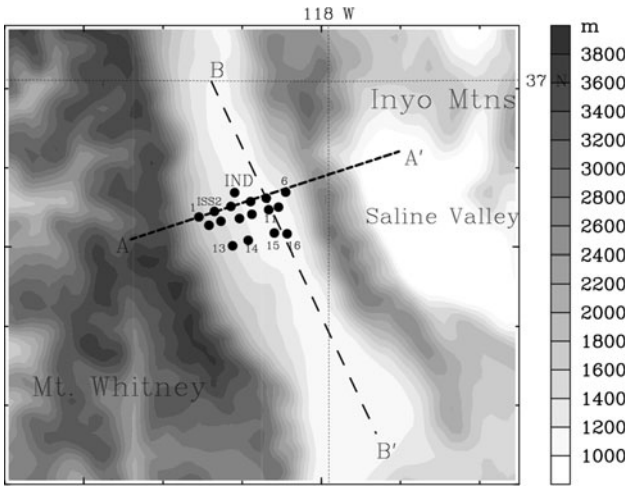

Fig. 2 Terrain feature (every 200 m) of the Owens Valley. The *dash lines* AA′ and BB′ represent the orientation of the *x–z* cross section in subsequent analyses. The *dots* denoted the 16 surface stations operated by the Desert Research Institute. *First row* is for station 1–6, *second row* is for station 7–12, and *third row* is for station 13–16. *IND* represents the Independence airport where the sounding was launched by the University of Leeds

Table 2 Owens Valley DRI Stations as shown in Fig. 2

Station	Elev (ft)	Elev (m)	Lat. (°)	Lon. (°)
01	5,697	1,710.2	36.76843	−118.27606
02	4,842	1,475.0	36.77777	−118.24322
03	4,180	1,274.1	36.78646	−118.20786
04	3,838	1,169.8	36.79470	−118.16616
05	3,756	1,144.8	36.80068	−118.13285
06	3,989	1,215.8	36.81095	−118.09142
07	5,165	1,574.3	36.75418	−118.25437
08	4,724	1,439.9	36.76099	−118.22916
09	4,061	1,237.8	36.76578	−118.18963
10	3,868	1,179.0	36.77298	−118.16334
11	3,761	1,146.4	36.78082	−118.12742
12	3,731	1,137.2	36.78521	−118.10654
13	4,724	1,439.9	36.71930	−118.20414
14	4,044	1,232.6	36.72855	−118.17111
15	3,727	1,136.0	36.74115	−118.11564
16	3,728	1,136.3	36.73974	−118.08823

down-valley wind system and especially the nocturnal LLJ is reproduced. Special attention will be paid to the importance of vertical resolution, choice of WRF boundary layer/surface physics, horizontal resolution, and accurate capturing of synoptic flow conditions.

Section 2 discusses the model and experimental design. Section 3 provides discussions of the EOP4 meteorology (based on analysis of observations). Section 4 discusses WRF control simulation results (including those of 3 variant model runs from the control) and includes results from an additional special four-nest simulation which was executed, and Sect. 5 offers conclusions.

2 Description of WRF model configuration and setup

The EOP4 of the T-REX was conducted from 2300 UTC 28 to 2000 UTC 29 April 2006 across the Owens Valley in southeastern California, surrounded by the Sierra Nevada Mountains to the west and the Inyo and White Mountains to the east. The White and Sierra Nevada Mountains each has peak elevations above 4 km asl, and the Inyo Mountains over 3.3 km asl. The average width of the valley is about 20 km (west to east), and its length about 120 km (southeast to northwest). Although the valley is a relatively elevated (1.2 km asl) endorheic basin, the great heights of its bounding mountain ranges make it one of the deepest valleys in the United States. There exist gaps and breaks (especially along the White and Inyo) where mid-level flow from outside the valley can penetrate in, and the valley floor is prone to a complex combined influence of (1) downward momentum transport of geostrophic winds from

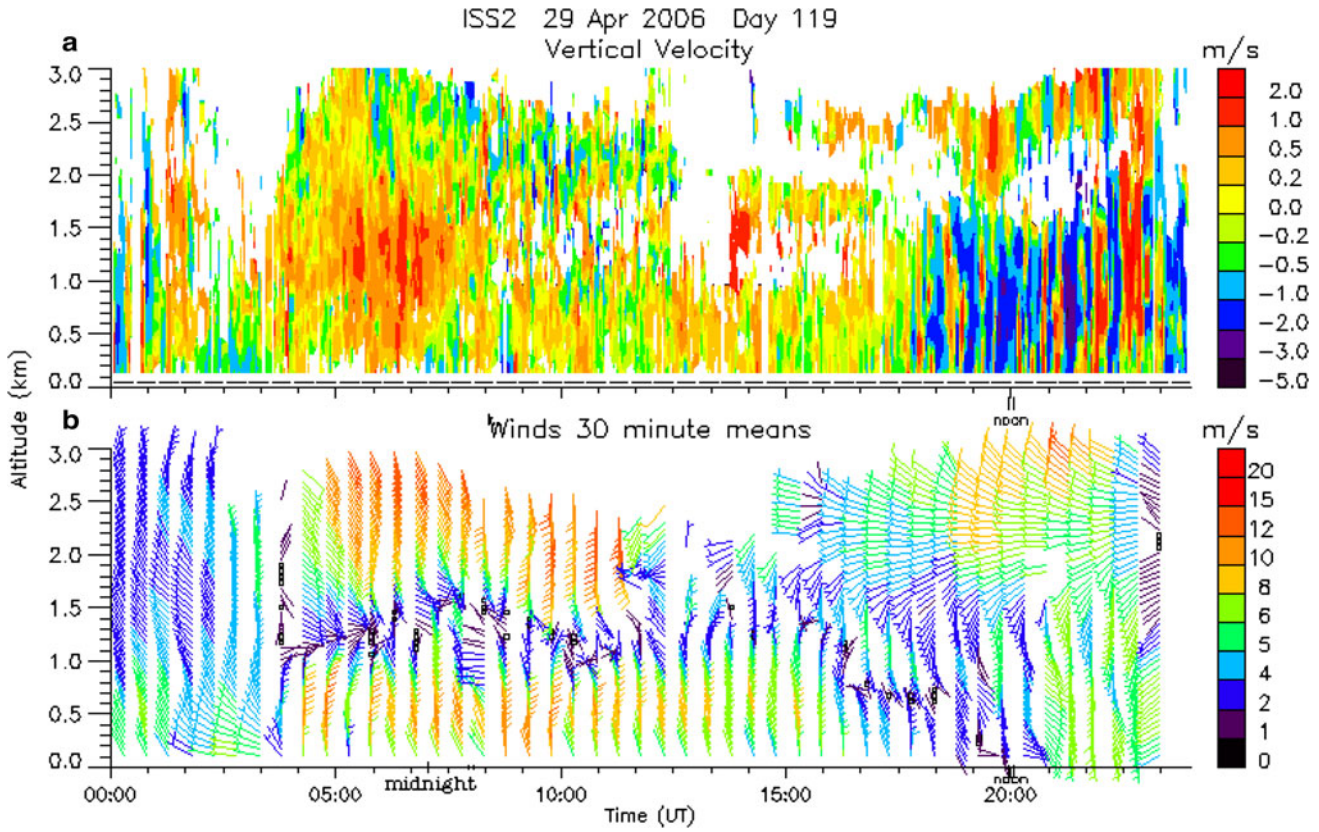

Fig. 3 ISS2 analysis of **a** vertical velocity (m s^{-1}) and **b** wind profiles (m s^{-1}) on 29 April 2006

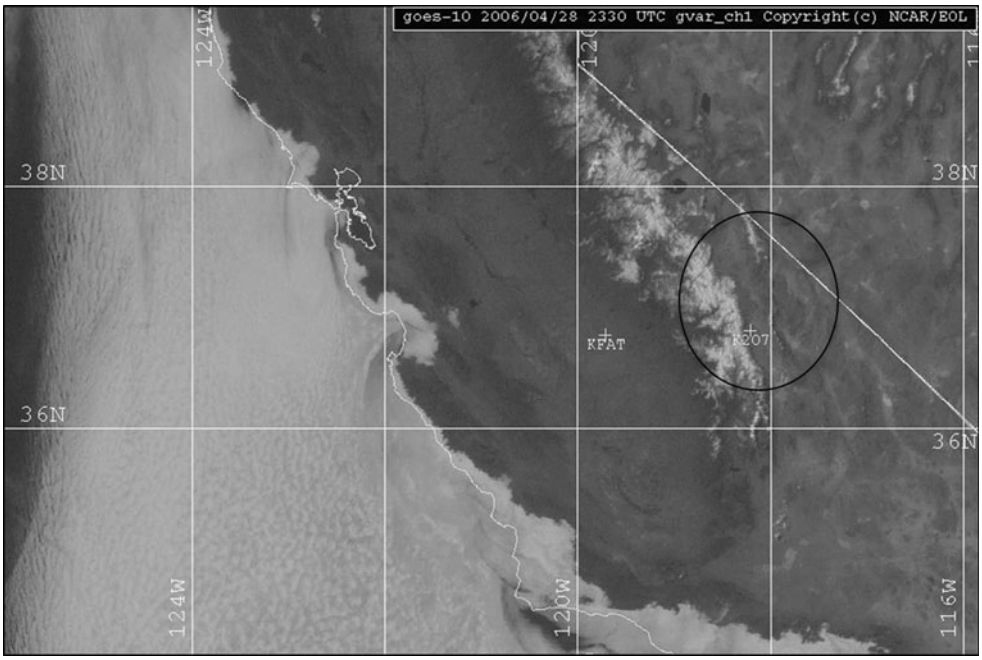

Fig. 4 GOES-10 1-km resolution visible imagery on 2330 UTC 28 April 2006

aloft, (2) pressure channeling (which can be offset 90° in direction from the geostrophic wind aloft), and (3) thermodynamically forced upslope/drainage and up-valley/down-valley flows (Schmidli et al. 2009).

A control simulation using a two-nest configuration with 4.5 km (121 × 121) and 1.5 km (169 × 169) grid spacing (Fig. 1) was executed, using 90 vertical terrain-following levels. This nesting configuration is similar to those which

have been tested at ARL for rapid update cycle nowcast purposes, although the vertical resolution is enhanced in this control setup. Sensitivity experiments varying both planetary boundary/surface layer physics and vertical resolution from the control run were also executed. The USGS 30 arc second database is used to generate the model topography and land use, applying 4-point averaging and a single-pass smoothing. In the 90 vertical level configuration, 24 of these are within the lowest 1 km agl. This vertical layer configuration (first 25 half-levels) is shown in Table 1 (as well as for the 60 vertical level variant). The initial conditions and time-dependent lateral boundary tendencies for the outer nest were provided by the North American Model (NAM) 12 km grid spacing forecasts produced by the National Center for Environmental Prediction (Janjic et al. 2001). No four-dimensional data assimilation is applied, so a 36-h simulation is conducted starting at 1200 UTC 28 April 2006 to allow for 12 h of mesoscale "spin-up" from the NAM cold-start initial conditions. The spin-up period allows mesoscale features to develop in the simulation (especially those due to topography) and dampens initial noise introduced through the interpolation of the NAM 218 (i.e., 12 km grid spacing) data onto the higher spatial resolution WRF grids.

For planetary boundary layer (PBL) and surface layer physics, the Quasi-Normal Scale Elimination (QNSE) scheme is employed in this study for the control run because it was specifically developed for stable stratification conditions. It is based on a 2.5 level closure and similar to the Mellor-Yamada-Janjic (MYJ) scheme in neutral-unstable conditions (Janjic 2001). In stable conditions, the QNSE is activated with turbulent eddies and waves treated as one entity within the stable regime. The QNSE accommodates the stratification-induced disparity between the transport processes in the horizontal and vertical directions and accounts for the combined effect of turbulence and waves. The model is based on a quasi-Gaussian mapping of the velocity and temperature fields. Details of the QNSE theory are described in Sukoriansky et al. (2005, 2006) and Galperin et al. (2007, 2008).

Elsewhere within the model, the atmospheric radiation schemes used are the rapid radiative transfer model (RRTM) (Mlawer et al. 1997) for the long wave, and for short wave transfers and interactions with the atmosphere, clouds, and the surface the scheme of Dudhia (1989) is used. In addition, terrain slope and shading effects on the solar radiation are taken into account. No cumulus parameterization option is used on both the 4.5 and 1.5 km nests. All convective and microphysical processes are resolved explicitly using the Thompson microphysical parameterization (Thompson et al. 2004). The Noah land-surface model (Chen and Dudhia 2001) option is also used.

3 The observed and modeled evolution of the down-valley flow

The 16 surface mesonet stations operated by the Desert Research Institute (DRI) are used for reconstructing surface wind and temperature analyses every 3 h throughout EOP4. There are three general W-E rows of DRI surface stations (Fig. 2) sited in the valley near the town of Independence. Also shown in Fig. 2 are zonal (AA′) and meridional (BB′) cross sections through the Owens Valley which are used for providing upper-level WRF simulation analyses. A list of the DRI stations is shown in Table 2.

Illustrating flow features above the Owens Valley throughout the evolution of the event, Fig. 3 depicts vertical velocity and wind profiles observed by the National Center for Atmospheric Research (NCAR) Integrated Sounding System (ISS) from 0000 UTC 29 to 0000 UTC 30 April. It is cautioned that the ISS2 measurements are likely contaminated from the flight pattern of migratory nocturnal birds during the overnight hours (Schmidli et al. 2009). High ISS2 profiler signal-to-noise ratios at these levels/times (not shown) are reliable indicators that such contamination occurred. Therefore, the ISS2 observations may not represent the nighttime flow situation accurately for heights in the vicinity of 1,000–2,000 m agl.

Both Figs. 4 and 5 show the synoptic weather conditions present during EOP4, governed by (1) an inverted trough passing through the Owens Valley by 1200 UTC 29 April

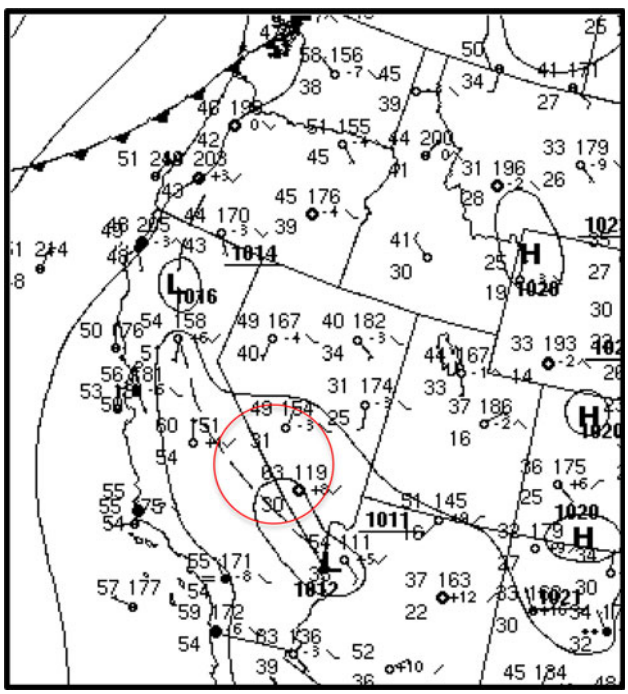

Fig. 5 Surface analysis at 1200 UTC (0500 LST) April 29 2006

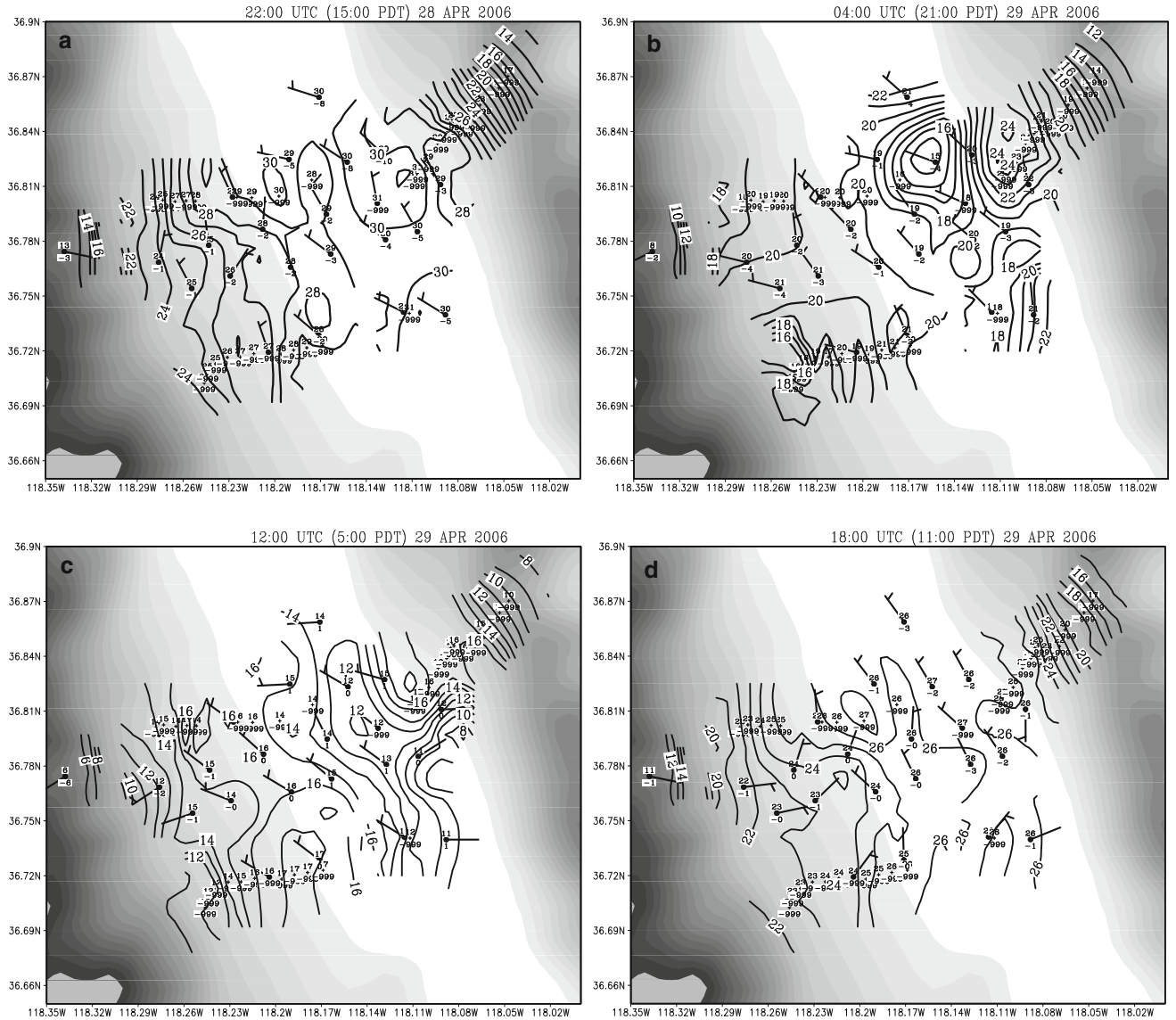

Fig. 6 Surface station analyses (T, Td, Wind speed, and Wind direction) valid at **a** 2200 UTC 28, **b** 0400 UTC 29, **c** 1200 UTC 29, and **d** 1800 UTC 29 April 2006. *Solid lines* denoted temperature contours (every 1 °C)

2006 behind a departing upper low and (2) a weak surface area of low pressure near the south end of the Owens Valley. This pattern produced moderate northerly mid- and upper-level geostrophic wind conditions over the region during the morning and afternoon of 28 Apr, weakening after midnight and eventually becoming southwesterly during the day of 29 Apr. In the very early morning hours of 28 Apr, the flow aloft may have been slightly more gradient than purely geostrophic. Atmospheric conditions were dry throughout (apparent clouds seen in Fig. 4 are actually snow cover over the Sierra Nevada Mountains).

The information provided by the surface analyses and the ISS2 profiles is enhanced through examining the WRF control simulation fields. The discussions in this study are based on the 1.5 km nest results. Figure 6 displays the EOP4 surface temperature and wind fields for different times throughout the EOP4 (based upon the DRI observations and objective analysis), while Fig. 7 shows the time evolution of these fields as produced by the WRF control simulation. To investigate boundary layer structure, cross sections BB′ and AA′ are constructed from the WRF control simulation displaying wind vector and wind component normal to the cross section (Figs. 8, 9). The BB′ meridional cross section is referred to hereafter as MCRS, while that of the zonal cross section AA′ as ZCRS.

Prior to 1800 UTC 28 April, the region was under strong synoptic forcing on the westward edge of a deep 500 hPa low moving into SE Arizona. Both observations and the WRF control simulation capture moderate NNE to NNW flow at this time at/above the 700 hPa level, in the vicinity

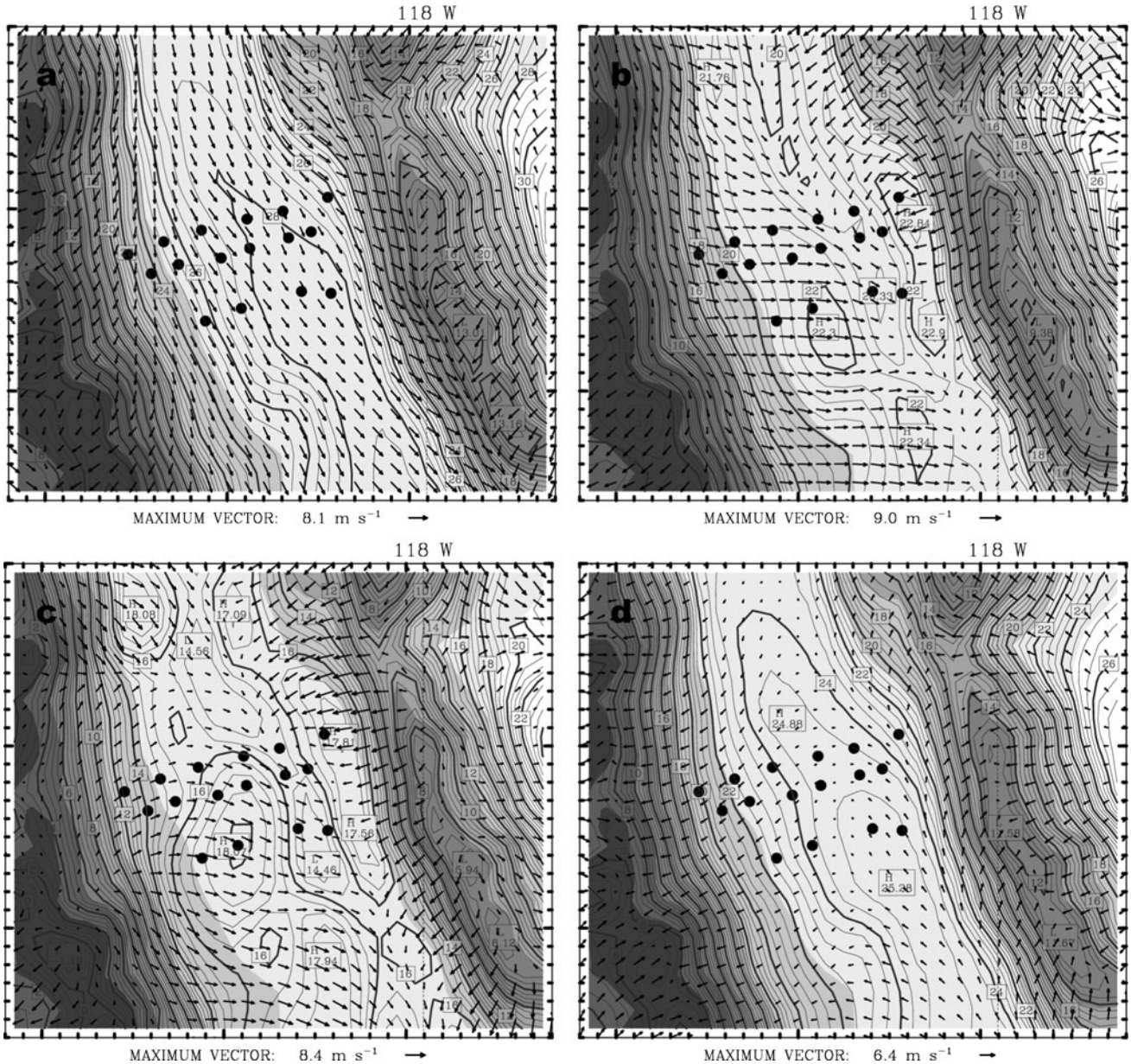

Fig. 7 Simulated 10-m wind (1 *full bar* 10 m s^{-1}) and 2-m temperature (°C; *dark gray contour*) from the control run valid at **a** 2200 UTC 28, **b** 0400 UTC 29, **c** 1200 UTC 29, **d** 1800 UTC 29 April 2006. *Shading color* denoted topography heights as shown in Fig. 1

of 12–15 m s^{-1}. At the surface, mostly northwest flow ($\sim$5 m s^{-1}) is observed by the DRI network at 2200 UTC 28 April (Fig. 6). The presence of afternoon down-valley flow is likely due to the synoptic forcing (other possible factors such as snow or cloud cover are absent), since southerly up-valley flow is preferred under weak synoptic forcing and the typical Owens Valley daytime differential heating. The north-northeast geostrophic flow at and above mountaintop level through the early evening of 29 April (UTC time) should have induced a pressure channeling effect near the valley floor favoring a northwest wind component.

Between 2200 UTC 28 and 0100 UTC 29 Apr, the ISS2 profiler, DRI observations, and the WRF control simulation continue showing a deep-layer north-northwest flow over the Owens Valley (Figs. 7, 8). The ZCRS (Fig. 9) shows a northerly 5–8 m s^{-1} meridional flow component in the lowest 1,000 m agl, with a secondary maximum above of about 2,500–3,000 m agl apparently associated with the synoptic geostrophic wind component. After 0100 UTC 29 April, west to west-northwest surface drainage flows ($\sim$5 m s^{-1}) initiated off the higher slopes of the Sierra Nevada. By 0400 UTC 29 Apr, the surface winds had increased to 7 m s^{-1} in areas of the western DRI network,

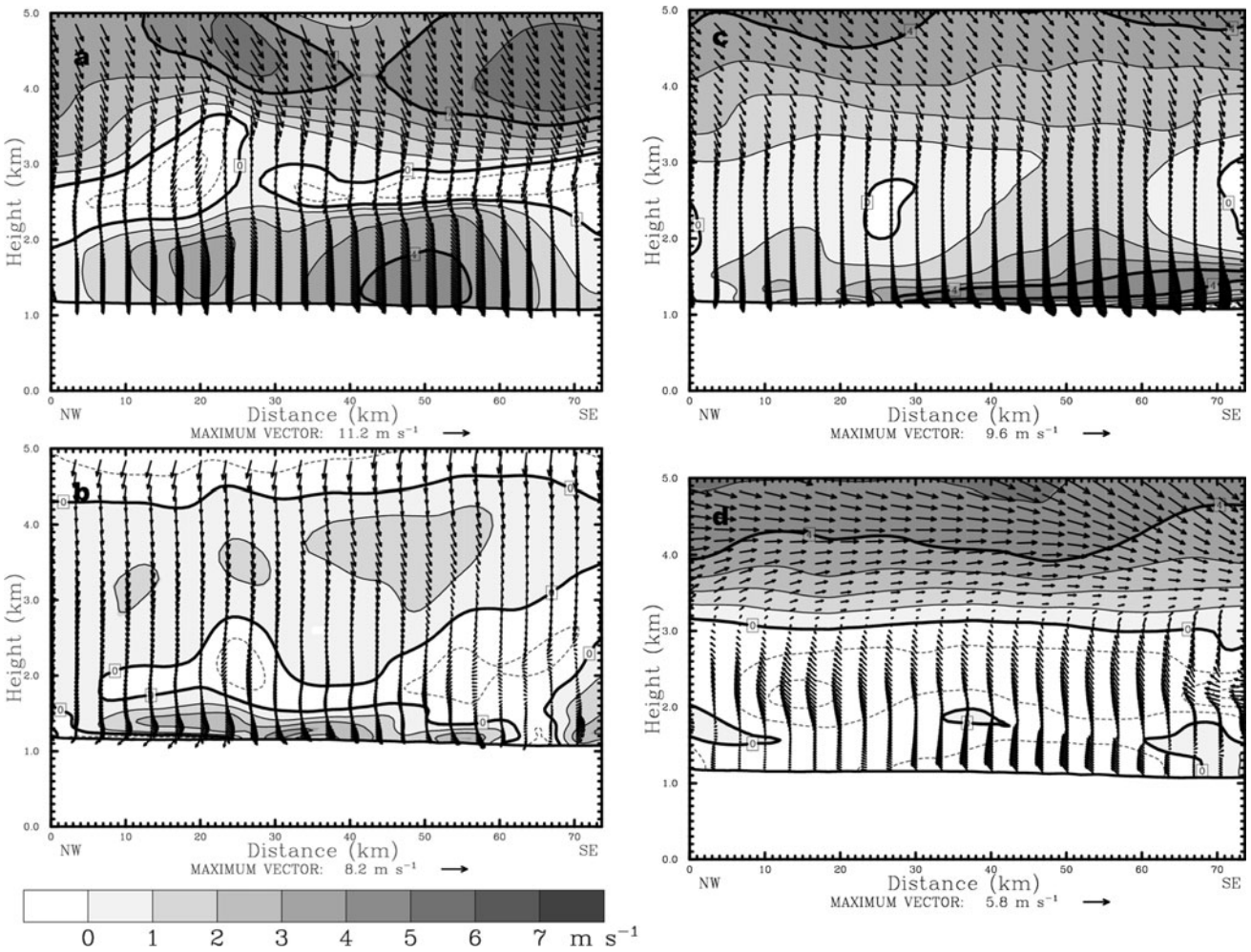

Fig. 8 Cross section of BB′ (NW–SE) showing the CTRL simulated horizontal wind component normal to the cross section (*shaded:* positive) and horizontal wind (vectors) from the 1.5 km domain valid at **a** 2200 UTC 28, **b** 0400 UTC 29, **c** 1200 UTC 29, **d** 1800 UTC 29 April 2006

with substantial drainage flows indicated along both the sidewalls of the Sierra Nevada and the Inyo Mountains (Figs. 6, 7). The WRF control simulation begins developing the nocturnal down-valley LLJ component with speeds of about 4–5 m s^{-1} over the middle of the Owens Valley, initially at around 300 m agl (Figs. 8, 9). This is consistent with observations from the ISS2 indicating LLJ strengthening through this period. Moreover, the ISS2 shows a sharp wind shift in direction and speed occurred below 1 km agl around 0400–0500 UTC (Fig. 3). This appears to be the initial period of development for the thermally driven nocturnal LLJ, as opposed to the purely synoptically driven LLJ observed earlier.

The northerly synoptic flow component aloft weakens nearing 0600 UTC 29 April, another hint that the invigorated down-valley LLJ is primarily due to valley mesoscale thermodynamic forcing after about 0400 UTC 29 Apr. The LLJ and stable inversion features are identifiable from the University of Leeds radiosonde soundings (Fig. 10) near Independence Airport (i.e., 1200 m above sea level), and initiate near the time of the wind shift around 0500 UTC 29 April. The LLJ also seems to originate first over the extreme western edge of the Owens Valley at the foot of the Sierra Nevada slopes (Fig. 7). The surface flow during this time (0400 UTC) of the nocturnal LLJ initiation remains generally west-northwest to northwest, although the WRF control simulation does produce stronger westerly drainage flows off the Sierra Nevada than observed by the DRI network.

The mature segment of the nocturnal LLJ occurs between 0700 and 1200 UTC of 29 April. The LLJ at around 500 m agl reaches a peak intensity around 0900–1000 UTC 29 Apr, thereafter slowly decreasing into the post-sunrise hours (i.e., weakening first in the northern end of the valley based on the simulation results). The WRF control simulation significantly underpredicts the maximum LLJ speed observed by the Independence radiosondes (Fig. 10) at certain times of the night, even

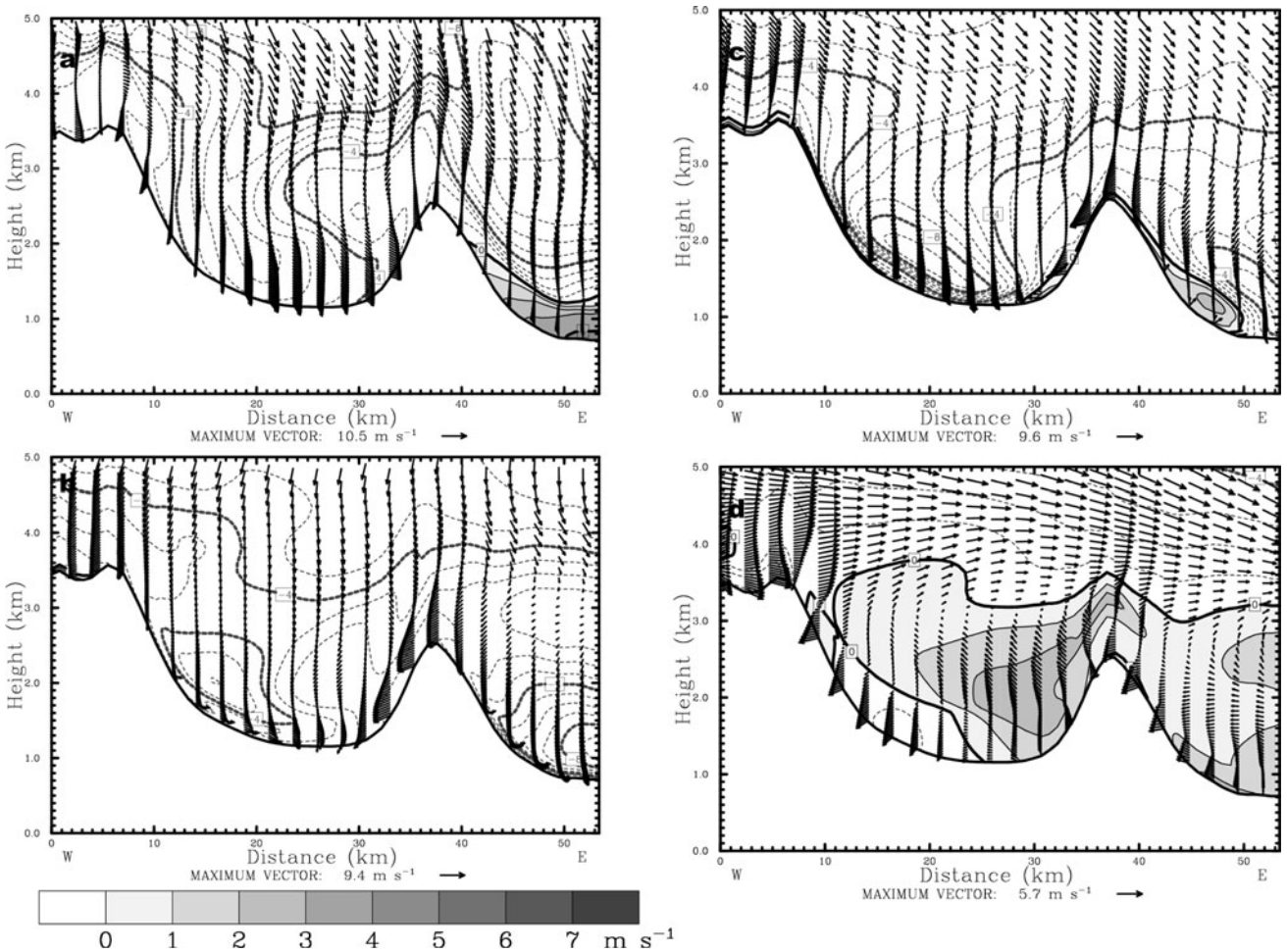

Fig. 9 Cross section of AA′ showing the CTRL simulated horizontal wind component normal to the cross section (*shaded*: positive) and horizontal wind (vectors) from the 1.5 km domain valid at **a** 2200 UTC 28, **b** 0400 UTC 29, **c** 1200 UTC 29, **d** 1800 UTC 29 April 2006

though it does reproduce the gross aspects and evolution of the nocturnal down-valley wind system quite well. The error in the total LLJ speed at 0900 UTC is up to 5–7 m s^{-1}. The 1200 UTC 29 April DRI observations (Fig. 6) show a valley surface cold pool ranging from about 12–14 °C, while the WRF control simulation carries a warm bias predicting more on the order of 14–15 °C (Fig. 7). Both MCRS (Fig. 8) and ZCRS (Fig. 9) also demonstrate the mature segment of nocturnal LLJ flow during this time.

The final segment of the LLJ is focused from 1500 UTC to 2100 UTC 29 Apr. The synoptic flow eventually turns to west-southwesterly by mid-morning of 29 April as the upper low moves to the vicinity of West Texas (ridging moves into the local area). Through the late morning of 29 Apr, the ISS2 low-level boundary layer flow remains consistently between about 6–12 m s^{-1} (Fig. 3). At 1800 UTC 29 Apr, the LLJ dissipates and a transition to surface up-valley and upslope flow begins (Fig. 6). The transition to up-valley flow appears to initiate first at higher levels after 1400 UTC 29 Apr, then works its way down towards the valley floor as the day progresses. This behavior is seen in both the ISS2 (Fig. 3) and the WRF control simulation (Fig. 7). By 2100 UTC 29 Apr, the down-valley flow transitioning to up-valley (southerly) flow is mostly complete, having begun initially at the valley's south end and then progressing northward (Figs. 8, 9). In addition, WRF output reveals that the nocturnal stable layer has elevated, and a well-mixed unstable boundary layer now exists (not shown).

4 Sensitivity experiments

4.1 Statistical comparisons of PBL schemes

The preceding section provided a mostly subjective analysis of the EOP4 Owens Valley meteorology using T-REX field observations and the 1.5 km WRF control simulation. This section offers a more objective evaluation of the WRF

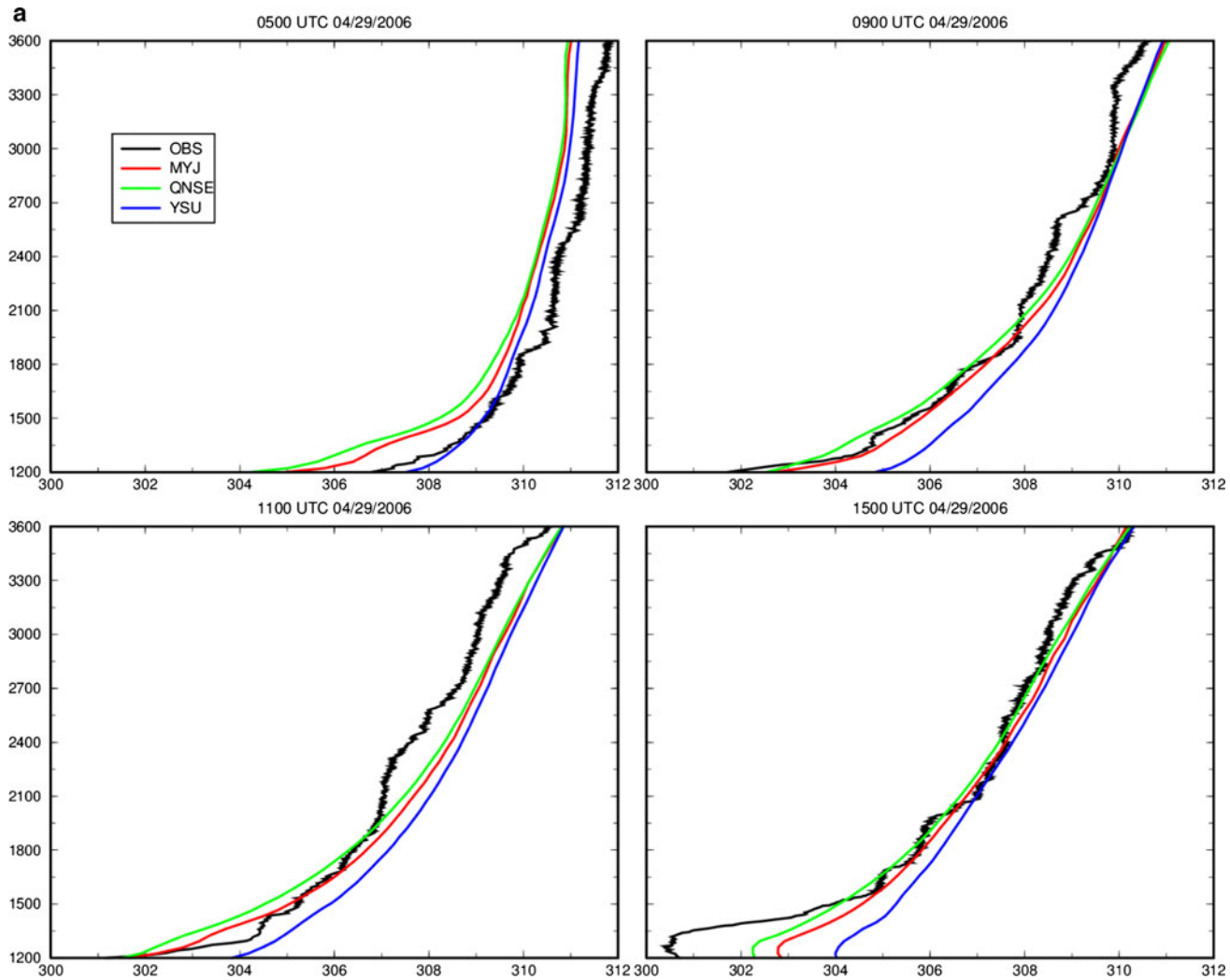

Fig. 10 Time evolution and comparison of **a** potential temperature profiles (K), **b** u-wind profiles (m s^{-1}) and **c** v-wind profiles (m s^{-1}) from model and sounding (*black*) at the Independence Airport (1,200 m above sea level)

performance throughout the EOP4. To perform a quick assessment of vertical resolution and planetary boundary/surface layer physics impacts of WRF in resolving the EOP4 meteorology, the model was run with additional member variants using the following modifications from the control configuration: the QNSE planetary boundary layer and surface physics with 60 instead of 90 vertical levels, the Yonsei State University (YSU) planetary boundary and surface layer physics with both 60 and 90 vertical levels, and the Mellor–Yamada–Jancic (MYJ) planetary boundary and surface layer physics with both 60 and 90 vertical levels. The QNSE scheme was discussed previously as it is used in the control configuration. In the MYJ scheme (Janjic 2001), the parameterization of turbulence in the PBL represents a non-singular implementation of the Mellor–Yamada Level 2.5 turbulence closure model (Mellor and Yamada 1982) through the full range of atmospheric turbulent regimes. In effect, the MYJ can be considered a "local" scheme. The YSU scheme is based on non-local mixing to include explicit entrainment fluxes of heat, moisture and momentum, counter-gradient transport of momentum, and different specification of the PBL height (Hong et al. 2006). It handles vertical diffusion with an implicit local scheme, and it is based on the local Richardson number in the free atmosphere.

The hourly mean observations collected from the 16 DRI surface mesonet sites are compared statistically to the 2 m agl WRF simulation temperature forecasts (for all WRF member variants and both nest resolutions). Table 3 displays some statistics including root mean square error (RMSE) and bias. The statistics were generated by (1) compositing across all 30 h of the simulation period over the 16 DRI stations, and (2) the same except the first 6 h of "spin-up" are eliminated. Eliminating the spin-up hours improves the overall statistical metrics as might be expected. The composite surface temperature statistics

Fig. 10 continued

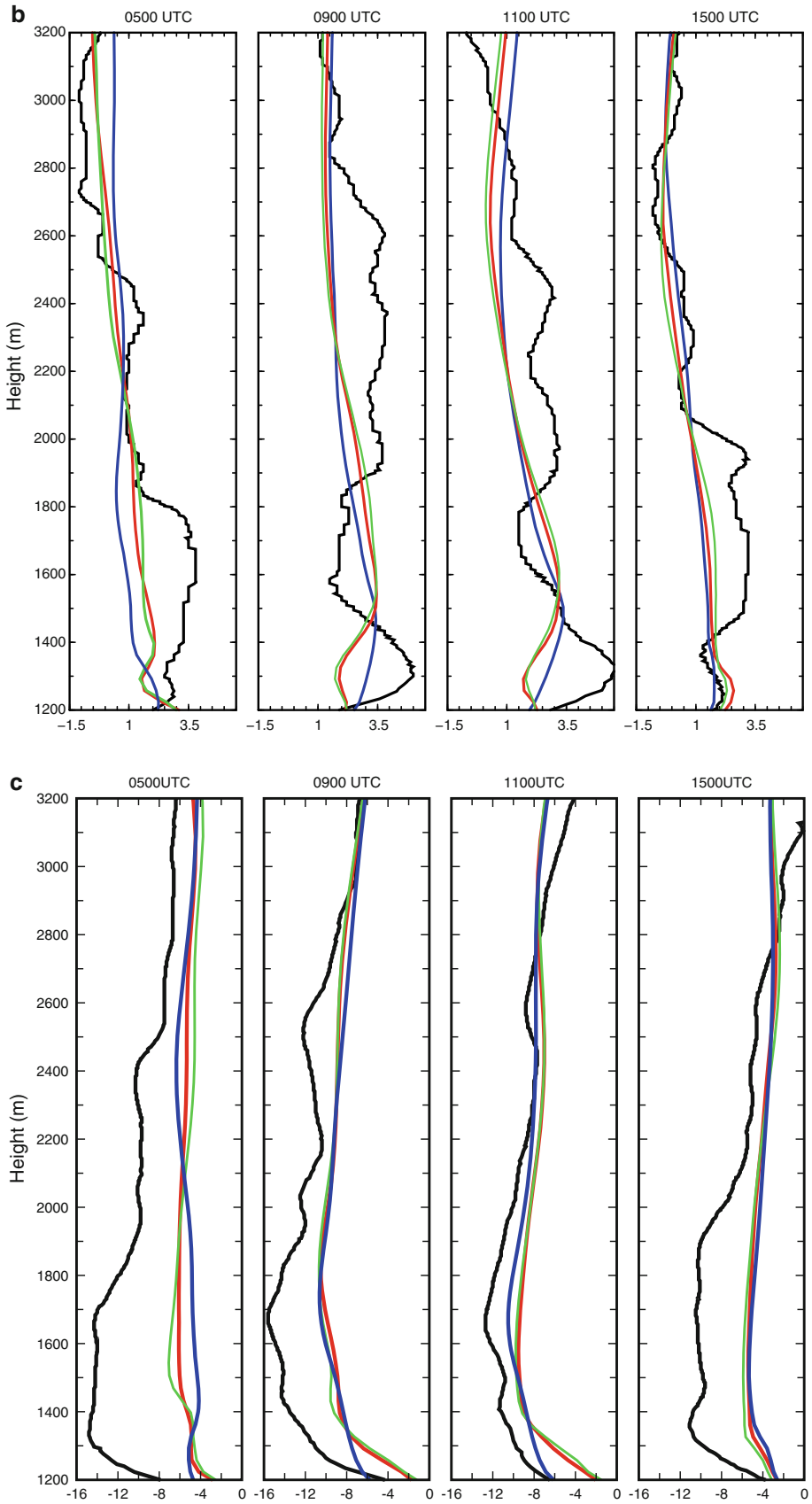

improve through the introduction of the finer horizontal grid spacing (1.5 km versus 4.5 km) as the local terrain differences are better resolved. The surface temperature statistics of the QNSE and MYJ PBL members are also improved from those of the YSU members throughout EOP4. When one examines the differences in the surface temperature results between using higher vertical resolution (90 vs 60 levels), very little improvement is noted.

In Fig. 10, the vertical profiles of potential temperature and wind for the same WRF simulations (other than the members using 60-vertical levels) are compared to radiosonde observations taken at the Independence Airport (i.e., 1,200 m asl). As noted in the previous section, all of the simulations underpredict the magnitude of the valley cold pool cooling by several deg C in the early post-sunrise hours. There is also a bit of a tendency for most members to over predict valley floor potential temperature cooling by several deg C in the mid-evening hours. Of interest is that the YSU member is clearly better with the near-surface potential temperature profile at 0500 UTC, although it is easily the worst performer at all other nighttime and early post-sunrise hours. Between 0900 and 1200 UTC, all of the member profiles are generally warm-biased above of about 600 m agl (i.e., 1800 m asl). The YSU member is warm-biased throughout the entire lower 2 km agl (i.e., 3.2 km asl) between these hours.

Using the same radiosonde observations, comparison of the u-wind component profiles (Fig. 10) shows some small variations between the three runs. The YSU member handles the u-wind profile over the lowest 200 m agl (1,400 m asl) slightly better, although the QNSE and MYJ predict more of the shallow ($\leq$50 m agl) early evening westerly slope component off the Sierra Nevada. All the simulations tend to underpredict the magnitude of the nocturnal u-wind component by roughly 1–2 m s^{-1}, although between 0900 and 1100 UTC there is also a period of slight u-wind over prediction by the simulations around 200–600 m agl (1,400–1,800 m asl).

Through analysis of the v-wind component (Fig. 10), we learn more about the WRF ability to resolve the nocturnal down-valley LLJ feature. All of the simulations predict the general overall evolution of the v-wind component within the PBL. The radiosonde observations show a somewhat trimodal nocturnal LLJ speed structure, with one peak around 150 m agl (1,350 m asl), a second around 500 m agl (1,700 m asl), and a third at about 1,200 m agl (2,400 m asl). After 0500 UTC, the simulations all tend to resolve one general extended peak in the v-wind component speed curve stretching between about 250–500 m agl (1,450–1,700 m asl). The YSU member also shows higher v-wind component speeds over the lowest 100 m agl between 0900 and 1100 UTC. None of the simulations resolve the upper peak near 1,200 m agl (2,400 m asl), which is probably more related to mid-level synoptic forcing.

The most significant finding from the radiosonde analyses is that there was a significant WRF under forecasting of the nocturnal LLJ speed magnitude, especially in the mid-late evening hours. This is clear in each of the three simulations. At some levels near 500 m agl (1,700 m asl), these total speed errors approach 6 m s^{-1} or greater. In fact, v-wind component errors were approaching 8 m s^{-1}. Based on the findings of the earlier paper of Schmidli et al. (2009), the LLJ model errors may be related to errors in resolving the mid-level forcing. The LLJ errors may also be partially due to having insufficient WRF spatial resolution (in their paper, adding an additional 300 m grid spacing nest improved LLJ speed slightly). The fact that 90 vertical levels are used in the simulations shown in Fig. 10 (14 levels within the lowest 500 m agl) makes vertical grid spacing an unlikely source for the EOP4 LLJ speed errors. Ongoing studies by Seaman et al. (2012) provide some useful guidance on the impact of model resolution in stable

Table 3 Statistical analyses for simulated surface temperature compared to the DRI 16 station observations

Domain/levels	16 DRI stations surface temperature statistical analysis						
	Total integration time (36 h)				Without first 6 h spin-up		
	Avg.	YSU	MYJ	QNSE	YSU	MYJ	QNSE
Dl 90	RMSE	2.8242	2.6457	2.4841	2.6598	2.4561	2.2903
Dl 90	BIAS	−1.5884	−1.2955	−1.1424	−1.2302	−0.8937	−0.7392
Dl 60	RMSE	2.895	2.6501	2.5474	2.7292	2.4676	2.3653
Dl 60	BIAS	−1.6851	−1.116	−1.0753	−1.3285	−0.6842	−0.6604
D2 90	RMSE	2.2387	1.8226	1.8709	1.9505	1.4193	1.4841
D2 90	BIAS	−1.1376	−0.9938	−1.0098	−0.6488	−0.4547	−0.4869
D2 60	RMSE	2.2617	1.811	1.8764	2.0016	1.4114	1.4969
D2 60	BIAS	−1.2463	−0.8256	−0.8348	−0.7654	−0.2572	−0.2795

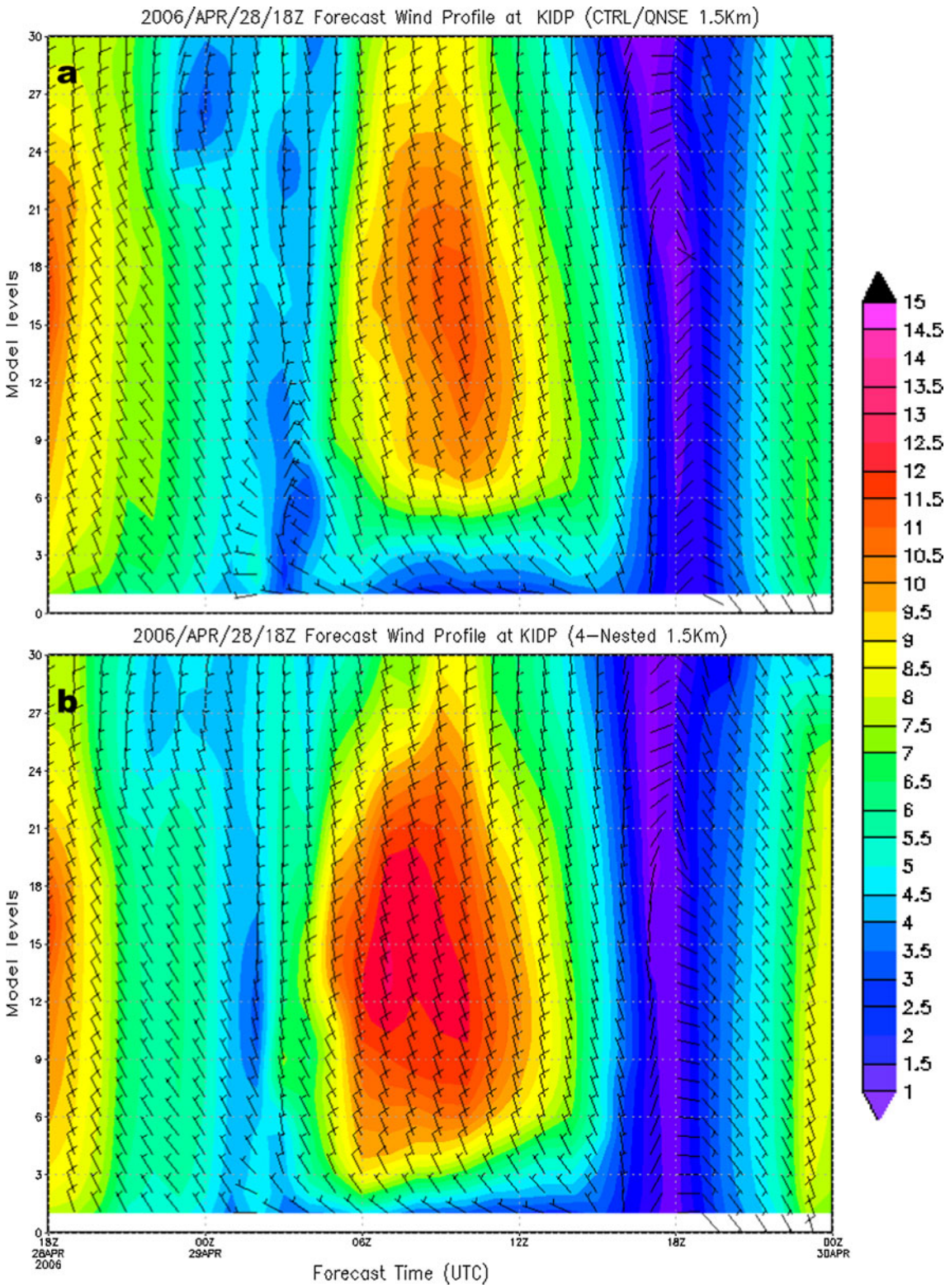

Fig. 11 Time evolution of the simulated low-level wind maximum at KIDP from 1.5 km domain of **a** QNSE (CTRL experiment), and **b** 4-nested experiment

stratification conditions. Variations in the choice of PBL and surface physics offered little change to the evolution of the gross EOP4 flow and LLJ features (except perhaps the YSU member in regards to flow within the lowest 100 m agl), although both the QNSE and MYJ members clearly outperformed YSU in reproducing the nighttime potential

temperature profile over the lowest few km agl. The remaining content of the paper attempts to lend credence to the idea that insufficient resolution of the upper/mid-level synoptic forcing is the primary source of the EOP4 nocturnal LLJ speed errors seen in the WRF runs just discussed.

Several results can be highlighted about the WRF simulations relative to their reproduction of the EOP4 meteorology: (1) the nocturnal down-valley LLJ was significantly underpredicted in magnitude; (2) other than a morning warm and mid-evening cold potential temperature bias at the lower levels, the gross surface and planetary boundary layer flow and thermodynamics are reproduced reasonably well (and better than the YSU) by both the QNSE and MYJ members; (3) the choice of planetary boundary/surface layer physics and using increased vertical resolution results in little improvement to predicting the nocturnal LLJ speed maximum; (4) increasing the horizontal resolution (4.5–1.5 km) results in better surface parameter statistics against the DRI mesonet observations. In addition, it can also be stated that the WRF member using the QNSE PBL/surface physics was not a clearly superior option (based on subjective and statistical comparisons) to the MYJ during the nocturnal hours under conditions of near-surface stable stratification. This was not necessarily expected based upon the literature related to QNSE. This raises some suspicion that the implementation of the QNSE in the WRF for stable conditions may have some existing deficiencies to address.

4.2 Sensitivity of four-nest simulation

Due to the previous results of Schmidli et al. (2009) and evolving from the previous discussions, one final additional WRF simulation was executed to examine the impacts of (1) improved large-scale synoptic forcing (through introduction of a courser resolution and larger outer nest), and (2) improved spatial resolution inside the valley (through introduction of an additional finer inner nest). The four-nest configuration used in this final simulation consists of 13.5 km, 4.5 km, 1.5 km, and 500 m nests. The 4.5 and 1.5 km nests are the same size/dimensions as used in the earlier two-nest configuration runs. The outer 13.5 km nest has dimensions of 121 × 121, while the inner 500 m nest has dimensions of 55 × 55. For vertical resolution, 90 levels were again used.

As can be seen in Fig. 11, it seems clear that the nocturnal low-level wind maximum (i.e., nocturnal LLJ) speed was predicted much closer to that observed by the radiosonde profiles (Fig. 10) using this four-nest configuration. This result suggested that the addition of the larger outer nest (i.e., 13.5 km) is the critical difference towards reproducing the more correct nocturnal LLJ speed maximum for EOP4. On the other hand, the additional 500 m inner nest does also seem to add a small amount of benefit. The formation of the valley cold air pool from nighttime to early morning is resolved much more accurately using the increased horizontal resolution of the 500 m nest (Figs. 6, 12). A couple of extra WRF simulations (not shown) ran in 13.5 km/4.5 km/1.5 km and 4.5 km/1.5 km/500 m configurations, and verified that the predominant improvement in predicting nocturnal LLJ speed is due to adding an additional (and larger areal coverage) 13.5 km outer nest. This finding is consistent with the that of Schmidli et al. (2009) that accurate treatment of the mid- and upper-level synoptic forcing conditions is a critical necessity to fully simulate Owens Valley LLJ and flow structure. For cold

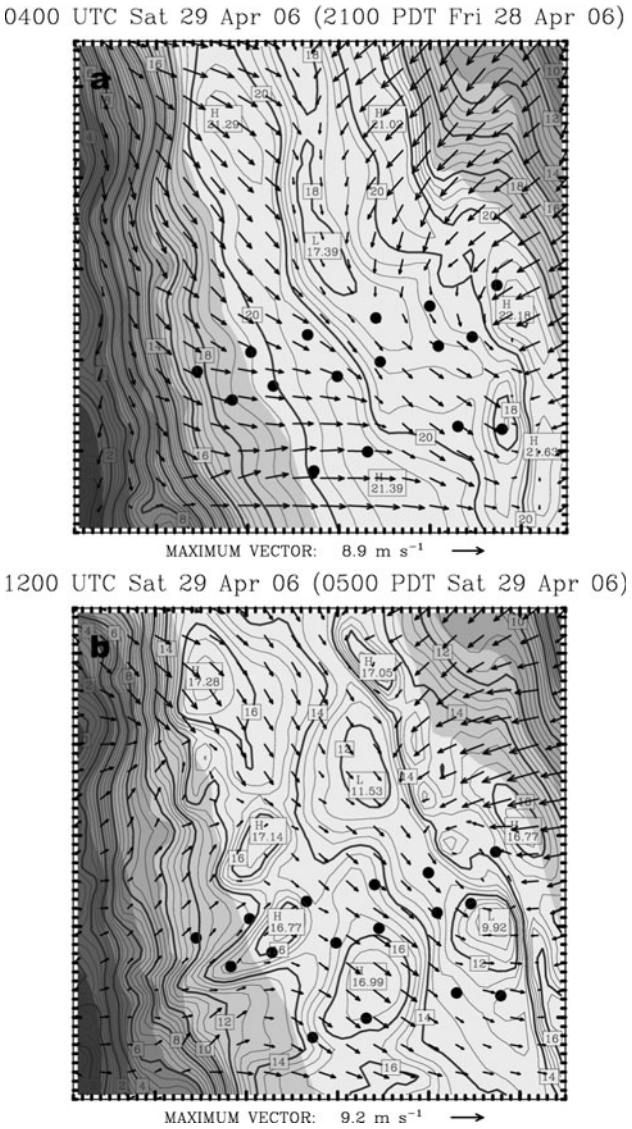

Fig. 12 The simulated cold air pool evolution from the 500 m domain of the 4-Nested experiment valid at **a** 0400 UTC 29 April and **b** 1200 UTC 29 April 2006

pool prediction, the horizontal resolution seems to play a much bigger role.

5 Conclusions

This study evaluated the WRF numerical weather prediction (NWP) model and its ability to simulate the EOP4 meteorology of the Owens Valley located in southern California. Special consideration was given to the evolution of the down-valley LLJ structure which was observed. A WRF control simulation (using 90 model levels and QNSE PBL/surface physics) produced reasonable gross meteorological flow and thermodynamic structures and their evolution, yet greatly under estimated the magnitude of the LLJ v-wind component. Since the Owens Valley down-valley LLJ is predominately meridional, the v-component speed is highly representative of the total LLJ speed. An additional WRF simulation based on the control except using 60 versus 90 model vertical levels showed that using the enhanced vertical resolution did not produce meaningfully different surface temperature bias and RMSE statistics. Two further WRF simulations, differing from the control only in using different options for planetary boundary/surface layer physics (YSU and MYJ rather than QNSE), also showed only minor differences in resolving the gross meteorological/statistical features of EOP4 and almost no improvement towards capturing the observed magnitude of the nocturnal LLJ speed max. Overall composite surface statistics seem to indicate a reasonable magnitude and range of error, when compared to the DRI surface observation network. The statistical results improve using the 1.5 km grid spacing nest versus the 4.5 km grid spacing nest, since terrain differences are much better resolved across the region. The statistical results are also better when the initial 6 h of model spin-up is eliminated in calculating the composites. This is likely due to several hours being required to bring the model fields into balance after initial "cold start" interpolation from the NAM to WRF grids. No data assimilation was applied. In addition, moist physics and snow cover were non-factors during EOP4.

The model vertical profiles of wind and potential temperature were also compared to the University of Leeds radiosondes released from the Independence Airport throughout EOP4. The potential temperature profiles for all the simulations displayed some larger errors of several degrees K near to the surface (mid-evening and just after sunrise), but generally they were reproduced adequately. The WRF wind profiles (for all members, including control) were simulated well in a gross sense, particularly the evolution and transitions associated with the EOP4 down-valley wind system. However, large errors of up to 7–9 m s^{-1} occurred in reproducing the low-level nocturnal jet v-wind (i.e., down-valley speed) component between about 100–500 m agl (1,300–1,700 m asl). Despite the magnitude errors in the nocturnal LLJ v-wind speed, both the WRF members reproduce an LLJ peak at about these same heights. The YSU member seems to capture the u-wind profiles a little closer to observations, except in the lowest 150 m agl or so where QNSE and MYJ do best in the evening. For both temperature and wind profiles, the QNSE PBL option did not prove to be a superior option to that of the MYJ during the nocturnal hours under stable stratification, which was a bit unexpected. This raises some suspicion that the implementation of the QNSE in the WRF for stable conditions may have some existing deficiencies to address.

One last additional four-nest WRF member was run, based on the control except adding two additional nests (an outer 13.5 km, and an inner 500 m), to test the idea that resolution of mid- and upper-level synoptic forcing might be critical to correctly resolving the key features of flow near the valley flow (such as LLJ). The results showed that the addition of the extra outer nest covering the larger areal extent (i.e., 13.5 km grid spacing nest) provided a substantially improved nocturnal LLJ speed max prediction. This seems consistent with previous research findings focused upon the Owens Valley and the T-REX EOPs (Schmidli et al. 2009). The additional finer resolution inner nest provided some very small improvement to the LLJ speed max prediction, but did provide a much improved cold pool representation in the early morning hours across the Owens Valley floor.

It is thought that use of data assimilation in the WRF for ingesting local surface and upper air observations (both valley interior, and external) might assist in further improving the EOP4 simulation of both local and regional conditions. Based on this study, the Army's proposed limited-area/high mesoscale resolution WRF nesting configuration(s) appears to be a reasonable approach for a rapid update nowcast system. This study also indicates the importance (within the ARL system) of providing not only accurate mesoscale initial and surface boundary conditions, but also lateral boundary conditions. This includes accurate treatment of mid- and upper-level forcing.

Acknowledgments The critical reviews of three anonymous reviewers were very helpful. The AWS data (DRI, HOBOs, and Leeds) were gathered as part of the Terrain-induced Rotor Experiment (T-REX). We acknowledge the suppliers of datasets employed here. Dr. William Brown at NCAR/EOL provides the ISS2 data and plotting software for Fig. 2. Discussions with Drs., Walter Bach, Semion Sukoriansky and Boris Galperin were appreciated. The research was supported by the Grant W911NF-09-1-0441 from the US Army Research Office.

References

Banta RM, Darby LS, Fast JD, Pinto JO, Whiteman CD, Shaw WJ, Orr BW (2004) Nocturnal low-level jet in a mountain basin complex. Part I: Evolution and effects on local flows. J Appl Meteorol 43:1348–1365

Chen F, Dudhia J (2001) Coupling an advanced land-surface/hydrology model with the Penn State/NCAR MM5 modeling system. Part I: Model implementation and sensitivity. Mon Weather Rev 129:569–585

Clements WE, Archuleta JA, Gudiksen PH (1989) Experimental Design of the 1984 ASCOT Field Study. J Appl Meteorol 28:405–413

Doran JC, Fast JD, Horel JD (2002) The VTMX 2000 campaign. Bull Am Meteorol Soc 83(4):537–551

Dudhia J (1989) Numerical study of convection observed during the winter monsoon experiment using a mesoscale two-dimensional model. J Atmos Sci 46:3077–3107

Dumais RE, Reen BP (2013) Data assimilation techniques for rapidly relocatable Weather Research and Forecast modeling. U.S. Army Research Laboratory Technical Note, ARL-TN-0546, July 2013

Galperin B, Sukoriansky S, Perov V (2007) Implementation of the quasi-normal scale elimination (QNSE) turbulence model in WRF. In: The 8th WRF Users' Workshop, Boulder, CO, June 11–15, 2007

Galperin B, Sukoriansky S, Atlaskin E (2008) Study of the effect of the QNSE-based surface layer parameterization on the warm bias in simulations of stably stratified boundary layers. In: The 18th symposium on boundary layers and turbulence, 9–13 June 2008, Stockholm, Sweden

Grubišić V, Doyle JD et al (2008) The Terrain-induced Rotor Experiment: an overview of the field campaign and some highlights of special observations. Bull Am Meteorol Soc 89:1513–1533

Gudiksen PH, Shearer DL (1989) The dispersion of atmospheric tracers in nocturnal drainage flows. J Appl Meteorol 22:602–608

Hong SY, Noh Y, Dudhia J (2006) A new vertical diffusion package with an explicit treatment of entrainment processes. Mon Weather Rev 134:2318–2341

Janjic ZI (2001) Nonsingular Implementation of the Mellor-Yamada Level 2.5 scheme in the NCEP meso model. National Centers for Environmental Prediction, Office Note #437

Janjic ZI, Gerrity JP, Nickovic S (2001) An alternative approach to nonhydrostatic modeling. Mon Weather Rev 129:1164–1178

Mellor GL, Yamada T (1982) Development of a turbulence closure model for geophysical fluid problems. Rev Geophys Space Phys 20:851–875

Mlawer EJ, Taubman SJ, Brown PD, Iacono MJ (1997) Radiative transfer for inhomogeneous atmospheres: RRTM, a validated correlated-k model for the longwave. J Geophys Res 102:16663–16682

Mursch-Radlgruber E (1995) Observations of flow structure in a small forested valley system. Theor Appl Climatol 52:3–17

Papadopoulos KH, Helmis CG (1999) Evening and morning transition of Katabatic flows. Bound Layer Meteorol 92:195–227

Pattantyus A, Dumais RE Jr (2013) Investigating lateral boundary forcing of Weather Research and Forecasting (WRF) model forecasts for artillery mission support. U.S. Army Research Laboratory Technical Memorandum, ARL-MR-0835, January 2013

Pinto JO, Parsons DB, Brown WOJ, Cohn S, Chamberlain S, Morley B (2006) Coevolution of down-valley flow and the nocturnal boundary layer in complex terrain. J Appl Meteorol Climatol 45(10):1429–1449

Princevac M, Hunt JCR, Fernando HJS (2008) Quasi-steady katabatic winds on slopes in wide valleys: hydraulic theory and observations. J Atmos Sci 65:627–643

Schmidli J, Poulos GS, Mobbs S (2007) T-REX EOPs III: Mesoscale valley circulations and sensitivity to synoptic conditions. In: Proceedings of the 29th international conference on alpine meteorology, Chambery, Meteo-France, 4–8 June 2007

Schmidli J, Poulos GS, Daniels MH, Chow FK (2009) External influences on nocturnal thermally driven flows in a deep valley. J Appl Meteorol Climatol 48:3–23

Seaman NL, Gaudet BJ, Stauffer DR, Mahrt L, Richardson SJ, Zielonka JR, Wyngaard JC (2012) Numerical prediction of submesoscale flow in the nocturnal stable boundary layer over complex terrain. Mon Wea Rev 140:956–977. http://dx.doi.org/10.1175/MWR-D-11-00061.1

Skamarock WC, Klemp JB, Dudhia J, Gill DO, Barker DM, Duda M, Huang XY, Wang W, Powers JG (2008) A description of the advanced research WRF Version 3 NCAR Technical Note, 2008

Sukoriansky S, Galperin B, Staroselsky I (2005) A quasi-normal scale elimination model of turbulent flows with stable stratification. Phys Fluids 17:85–107

Sukoriansky S, Galperin B, Perov V (2006) A quasi-normal scale elimination model of turbulence and its application to stably stratified flows. Nonlinear Process Geophys 13:9–22

Thompson G, Rasmussen RM, Manning K (2004) Explicit forecasts of winter precipitation using an improved bulk microphysics scheme. Part 1: description and sensitivity analysis. Mon Weather Rev 132:519–542

Triantafyllou AG, Helmis CG, Asimakopoulos DN, Soilemes AT (1995) Boundary layer evolution over large and broad mountain basin. Theor Appl Climatol 52:19–25

Whiteman CD, Zhong S (2008) Downslope flows on a low-angle slope and their interactions with valley inversions. Part I: Observations. J Appl Meteorol Climatol 47:2023–2038

Whiteman CD, McKee TB, Doran JC (1996) Boundary layer evolution within a canyon land basin. Part I. Mass, heat, and moisture budgets from observations. J Appl Meteorol 35:2145–2161

Whiteman CD, Hoch SW, Poulos GS (2009) Evening temperature rises on valley floors and slopes: their causes and their relationship to the thermally driven wind system. J Appl Meteorol Climatol 48:776–788

Zhong S, Whiteman CD (2008) Downslope flows on a low-angle slope and their interactions with valley inversions. Part II: Numerical modeling. J Appl Meteorol Climatol 47:2039–2057

Zumpfe DE, Horel JD (2007) Lake-breeze fronts in the Salt Lake Valley. J Appl Meteorol Climatol 46:196–211